Article:
Hua, Y, Barker, RJ and Neville, A (2015) The effect of O2 content on the corrosion behavior of X65 and 5Cr in water-containing supercritical CO2 environments. Applied Surface Science, 356. pp. 499-511. ISSN 0169-4332

https://doi.org/10.1016/j.apsusc.2015.08.116

The effect of O_2 content on the corrosion behavior of X65 and 5Cr in water-containing supercritical CO_2 environments

Yong Hua, Richard Barker and Anne Neville

Institute of Functional Surfaces

School of Mechanical Engineering

University of Leeds

Leeds

LS2 9JT

United Kingdom

Corresponding author: Yong Hua, Tel: +44 (0) 7923359918, fax: +44 (0) 1132424611.

Email: leo.huayong@gmail.com

ABSTRACT

The general and localized corrosion behavior of X65 carbon steel and 5Cr low alloy steel were evaluated in a water-saturated supercritical CO_2 environment in the presence of varying concentrations of O_2. Experiments were performed at a temperature of 35℃ and a pressure of 80 bar to simulate the conditions encountered during CO_2 transport and injection. Results indicated that increasing O_2 concentration from 0 to 1000 ppm caused a progressive reduction in the general corrosion rate, but served to increase the extent of localized corrosion observed on both materials. Pitting (or localized attack) rates for X65 ranged between 0.9 and 1.7 mm/year, while for 5Cr rose from 0.3 to 1.4 mm/year as O_2 concentration was increased from 0 to 1000 ppm. General corrosion rates were over an order of magnitude lower than the pitting rates measured. Increasing O_2 content in the presence of X65 and 5Cr suppressed the growth of iron carbonate ($FeCO_3$) on the steel surface and resulted in the formation of a corrosion product consisting mainly of iron oxide (Fe_2O_3). 5Cr was shown to offer more resistance to pitting corrosion in comparison to X65 steel over the conditions tested. At concentrations of O_2 above 500 ppm 5Cr produced general corrosion rates less than 0.04 mm/year, which were half that recorded for X65. The improved corrosion resistance of 5Cr was believed to be at least partially attributed to the formation of a Cr-rich film on the steel surface which was shown using X-ray photoelectron spectroscopy to contain chromium oxide (Cr_2O_3) and chromium hydroxide ($Cr(OH)_3$). A final series of tests conducted with the addition of 1000 ppm O_2 in under-saturated conditions (water content below solubility limit) revealed that no corrosion was observed when the water content was below 1200 ppm for both materials.

Keywords: supercritical CO_2, corrosion, CCS, iron carbonate, iron oxide, oxygen,

INTRODUCTION

The carbon capture and storage (CCS) process requires efficient, safe and cost effective methods for the transport of carbon dioxide (CO_2) from its point of capture to the site of sequestration[1]. In terms of the transport of CO_2, carbon steel pipelines are generally the most practical solution, particularly over long distances[1] and it is likely that the majority of such pipelines will operate under high pressure to ensure CO_2 is transported in a supercritical state (or dense phase), maintaining favorable flow characteristics to facilitate cost effective transport. This supercritical state can be achieved by transporting CO_2 at conditions above its critical temperature and pressure of 31°C and 73.8 bar, respectively[2, 3].

Given that future high pressure CO_2 pipelines may be placed in densely populated areas, it is of paramount importance that they are safe to operate and do not present a hazard to the surrounding population. One risk that needs to be understood is the threat of internal corrosion of the pipelines when free water is present within the system, as this facilitates the formation of carbonic acid (H_2CO_3). The presence of CO_2 and water alone can result in the formation of a low pH aqueous phase (~pH of 3.1 based on simulations performed by Ayello at high pressure[2]) which can be particularly aggressive towards carbon steels. Furthermore, there is also the possibility of other contaminants existing in the CO_2 stream which can influence and potentially accelerate the corrosion process. These impurities depend upon the combustion source, the capture technique employed and the level of gas treatment/purification implemented during the CCS process. However, it is anticipated that in addition to CO_2 and water, the process fluid may contain traces of sulphur dioxide (SO_2), nitrogen oxides (NO_x), carbon monoxide (CO), hydrogen sulphide (H_2S), methane (CH_4) and oxygen (O_2) to name a few. Understanding the effects of such impurities on the corrosion process is of paramount importance to ensure the safe transport of dense phase CO_2 during the CCS process.

Considering all the potential impurities, the water content is the most critical factor in terms of influencing both the occurrence and extent of corrosion. Consequently, measures are taken to remove water down to levels below the solubility limit in dense phase CO_2. Regrettably, this process can be costly, and there is no general consensus on the actual water content or relative humidity required to prevent corrosion or reduce it to appreciable levels. Determining the influence of the water content on pipeline integrity in the presence of the different natural and anthropogenic impurities in high pressure CO_2 environments has recently been the subject of significant research efforts[4, 5, 6, 7, 8, 9].

In this work, our aim was to complement the existing literature by systematically reviewing the influence of O_2 on the corrosion of X65 carbon steel and 5Cr in supercritical CO_2

environments. Although the influence of O_2 content on CO_2 corrosion is not a new subject area and has been investigated a number of decades ago in systems relevant to oil and gas production, little is known about the effects of this particular impurity in CO_2 streams that are typical of those used in CCS[10].

In the context of oil and gas transportation and seawater injection, the presence of O_2 in CO_2 corrosion systems has been reported to have a two-fold effect on corrosion behavior; firstly, by introducing an additional cathodic reaction (for acidic solutions)[11], which can potentially accelerate the level of corrosion:

$$O_2 + 4H^+ + 4e^- \rightarrow 2H_2O \quad (1)$$

and secondly, through the ability of O_2 to inhibit the formation of protective iron carbonate ($FeCO_3$) by oxidising ferrous ions to ferric ions, resulting in the formation of what has been suggested to be a non-protective iron oxide film[3, 12]. However, other observations in literature have suggested that O_2 was able to 'enhance' the formation of $FeCO_3$ under oil and gas conditions, generating a protective film which produced no indications of localized corrosion of the underlying steel[13].

Although limited, the influence of O_2 on the corrosion behavior of carbon steels in water-containing dense phase CO_2 has been considered in literature. Work by Choi et al.,[3] showed that general corrosion rates of X65 increase from 0.38 to ~1.05 mm/year in conjunction with a rise in O_2 content from 0 to 4% in a water-saturated supercritical CO_2 phase at 80 bar and 50°C. However, the O_2 concentrations evaluated in their study could be argued to be much higher than those typically expected during normal CO_2 service as well as being much greater than the recommended O_2 levels provided in tentative specifications for CO_2 purity (as will be discussed later)[14, 15].

In a separate study, Choi and Nesic[8] also showed that under the same operating conditions in the presence of 2.5% O_2, water contents of 3000 ppm and below were all shown to produce general thickness loss rates less than 0.1 mm/year, suggesting that the presence of O_2 in conjunction with only water and CO_2 does not present a significant corrosive threat in terms of general corrosion, even at high levels of humidity in a dense phase system. Similar experiments were conducted by Zeng and co-workers[16] who considered the influence of O_2 content (1.4 and 2.8 bar partial pressures) and total pressure (77 to 103 bar) on the corrosion of carbon steel in water-saturated supercritical CO_2 at 35 and 45°C. Mass loss results showed that the uniform corrosion rate increases with total pressure from 76 bar to 103 bar, with the rate of thickness loss ranging from 0.02 to 0.13 mm/year after 5 days exposure. Zeng et al.,[16] suggested that there exists a threshold pressure of approximately

100 bar in the presence of O_2, beyond which there is a noticeable increase in general corrosion rate. However, one key point from both these studies is that the extent of localized corrosion within the system was not reported or quantified, which when reviewing the experience from the oil and gas industry may well be an important aspect to consider.

When consolidating the literature relating the effect of O_2 as an impurity in dense phase CO_2 on the corrosion of carbon steel, it is evident that research gaps still remain and that the role of O_2 is complex, with different observations existing in literature depending upon the conditions considered. It is clear from experiments replicating oil and gas production or seawater injection that O_2 can play a role in initiating localized attack on carbon and low alloy steels[3, 12, 13, 17], yet the potential for this to occur in dense phase transport systems appears to have not been evaluated in open literature. Consequently, the focus of this work was directed towards understanding the influence of O_2 content on the general *and* localized corrosion behavior of both X65 carbon steel and 5Cr steel in water-containing dense phase CO_2 systems.

EXPERIMENTAL PROCEDURE

Materials and preparation

Test specimens were machined from carbon steel (API 5L X65) and 5Cr low alloy steel (ASTM A182-F5) into discs of diameter 25 mm and thickness of 6 mm. The chemical composition of the X65 and 5Cr steels are provided in Table 1. Surface preparation consisted of wet-grinding the entire sample up to 600 grit silicon carbide abrasive paper, rinsing with distilled water, followed by acetone, high purity ethanol and drying gently with compressed air. Samples were then stored in a desiccator until required and weighed immediately before the experiment on an electronic balance with an accuracy of 0.01 mg, before suspending inside the autoclave. Two samples were placed within the autoclave for each individual test.

Autoclave testing procedure

A schematic representation of the autoclave experimental system layout has been shown in a previous publication.[18] The entire system consists of a 1 litre capacity autoclave, temperature controller, a CO_2/O_2 mixed cylinder, a liquid CO_2 cylinder and a series of valves for CO_2 flow control.

The distilled water used in each experiment was de-aerated by saturating the solution with CO_2 in a separate container for a minimum of 12 hours prior to testing. The specimens were suspended within the autoclave on a non-conducting wire whilst also ensuring they were not in contact with the walls of the cylinder to prevent galvanic effects. The prepared, CO_2-

saturated water was carefully delivered into the bottom of the autoclave at ambient pressure and temperature and sealed. All lines to the autoclave were then purged with CO_2 and evacuated to ensure the removal of initial traces of O_2 within the system. The required technical grade of CO_2/O_2 mixture and liquid CO_2 was then transferred into the autoclave, heated and pressurized to the correct temperature and pressure. The starting point of the test was taken from the time at which the autoclave reached the required temperature and pressure (35°C and 80 bar in this particular study).

All tests were conducted in static conditions in either water-saturated supercritical CO_2, or with the water content below the calculated solubility limit. According to Spycher et al.[19], the saturated water concentration in supercritical CO_2 at 35°C and 80 bar is 3437 ppm. In order to ensure the water-saturated CO_2 condition, 34000 ppm of water was introduced to the bottom of the autoclave (not in direct contact with the sample) for the water-saturated tests (i.e. approximately 10 times the saturation limit). The entire matrix of the experimental conditions is provided in Table 2, which describes the different O_2 and water contents that were evaluated.

At the end of each experiment, the specimens were dried thoroughly and photographed. The samples were subsequently chemically cleaned to remove all traces of corrosion products before weighing. The cleaning process consisted of wiping the surface with a cotton pad soaked in Clarke's solution (20 g antimony trioxide + 50 g stannous chloride + 1000 ml hydrochloric acid) in accordance with ASTM Standard G1-03[20]. This was followed by rinsing the samples with distilled water and then drying with compressed air.

The mass loss due to corrosion was determined from the weight difference before exposure and after cleaning. The corrosion rates were calculated by using Equation (2):

$$V_c = \frac{87600\Delta m}{\rho A t} \quad (2)$$

where V_c is the corrosion rate of the sample in mm/year, Δm is the weight loss in grams, ρ is the density of the sample in g/cm^3, A is the exposed area in cm^2 and t is the immersion time in hours.

Justification for selection of test conditions

The decision to evaluate O_2 concentrations between 0 and 1000 ppm was based on two tentative CO_2 purity recommendations within literature. These are from the European project 'ENCAP – ENhanced CAPture of CO_2[14], and a set of compiled data from Alstom which was referred to in a publication by Dugstad et al.[21]. In terms of concentration limits, the

recommended maximum concentration of O_2 for enhanced oil recovery (EOR) applications is <1000 ppm based on both specifications, although it is unclear how these particular limits were established. One assumes it is based on a concentration required to prevent undesirable exothermic reactions with hydrocarbons at the injection point during the EOR process.

It is perhaps worth noting that there is currently no universally agreed upon purity specification for CO_2 during dense phase transport, but it is clear that there is very little public data available relating to the localized corrosion behavior of carbon steels in dense phase CO_2 containing O_2 in the ranges recommended by DYNAMIS[14] and Alstom[21]. This lack of data was also pointed out in a recent review of corrosion in CO_2 transport by Halseid et al.[22].

RESULTS AND DISCUSSION

Carbon steel and 5Cr samples exposed to water-saturated CO_2 – effect of O_2 concentration

The general corrosion rates of X65 carbon steel and 5Cr in water-saturated CO_2 conditions at 35°C and 80 bar are provided in Figure 1. After 48 hours of exposure in the absence of O_2, general corrosion rates of 0.10 and 0.125 mm/year were recorded for X65 and 5Cr, respectively. As O_2 concentration was increased up to 1000 ppm, the general corrosion rate of both materials progressively reduced, reaching 0.04 and 0.02 mm/year for X65 and 5Cr, respectively. This data produces comparable results with the work of Zeng et al.,[16] who evaluated the corrosion behavior of carbon steels in the presence of 1.4 bar and 2.8 bar O_2. Their experiments in water-saturated CO_2 produced general corrosion rates of approximately 0.03 mm/year when an O_2 concentration of 1.4 bar was introduced to the system, aligning with the observed corrosion rates in the presence of 1000 ppm O_2 in Figure 1. In terms of tests in the absence of O_2, the corrosion rate of 0.10 mm/year for X65 corroborates with the work of Sim et al.[23] who recorded a general corrosion rate of 0.08 mm/year in water-saturated conditions at 80 bar and 40°C.

It may be expected that in the presence of an oxidiser such as O_2, the general corrosion rate of carbon steel would be expected to increase, however, this was not the case. Similar observations were made by Ayello et al.,[2] who performed tests on carbon steel at 75.8 bar and 40°C with the addition of 100 ppm O_2. Electrochemical measurements performed within an autoclave indicated that O_2 did not increase general corrosion rates. Furthermore, by combining experiments with equation of state modelling, Ayello and colleagues[2] were able

to show that the low concentration of O_2 and the low pH in the system (~3.1) may have limited the role of O_2 as a cathodic reactant. Furthermore, it was shown that O_2 had no influence on the pH of the aqueous phase in the system at a concentration of 100 ppm, as expected.

Figure 2 presents the photographs and scanning electron microscopy (SEM) images of the corroded X65 carbon steel samples exposed to the water-saturated conditions. Images of the steel surface exposed to 0 and 20 ppm O_2 (Figures 2(a) and 2(b)) indicate the presence of a crystalline $FeCO_3$ corrosion product on the steel surface. As O_2 content is increased to 1000 ppm, the quantity of visible crystalline $FeCO_3$ corrosion product on the steel surface reduced, as reflected in Figures 2(c) and (d). The presence of $FeCO_3$ on the surface of X65, as well as its suppression by increased levels of O_2 are confirmed for tests at 0, 20, 500 and 1000 ppm of O_2 by the XRD patterns provided in Figure 3, which exhibits clear peaks representative of siderite that reduce significantly in intensity as O_2 concentration increases. Figure 3 shows that the addition of 1000 ppm O_2 resulted in complete inhibition of $FeCO_3$ formation. In the presence of O_2, a proportion of the Fe^{2+} in the bulk solution will be oxidised to Fe^{3+}, which will inevitably reduce the concentration of Fe^{2+} available for $FeCO_3$ precipitation. This effect of O_2 on $FeCO_3$ formation has also been reported by Rosli et al.[12] who demonstrated that O_2 contents at low as 1 ppm can have a profound effect on CO_2 corrosion in aqueous environments at 80°C and pH 6.6 under atmospheric pressure. In their work, Rosli et al.[12] observed that O_2 presence resulted in a heterogeneous corrosion product forming on carbon steel under CO_2-saturated atmospheric conditions consisting of iron oxides and $FeCO_3$. These oxide deposits appeared to facilitate the propagation of localized corrosion directly underneath where they were situated on the steel surface.

Although the XRD patterns for 1000 ppm O_2 addition indicated no crystalline species on the steel surface, an orange/brown corrosion product was apparent on the surface of X65. Energy dispersive X-ray measurements in Figure 2(d) indicated that these products had an elemental composition which comprised of iron and oxygen, suggesting that iron oxides/hydroxides were present on the surface but were either amorphous in nature, or thin enough to elude detection by XRD. Both Rosli et al.[12] and Zeng et al.[16] made similar observations, with the latter authors performing experiments in supercritical CO_2 conditions. Rosli et al.[12] confirmed that the presence of O_2 resulted in the formation of magnetite (Fe_3O_4), goethite (FeOOH) and hematite (Fe_2O_3) through XRD measurements, while Zeng et al.,[16] suggested that O_2 resulted in the formation of Fe_2O_3 and Fe_3O_4 on the steel surface, although this was not confirmed through any spectroscopic techniques.

Photographs and scanning electron microscopy (SEM) images of the corroded 5Cr steel samples exposed to the conditions tested within the matrix in Table 2 are provided in Figure 4. The corrosion deposits observed in Figures 4(a), (b) and (c) are shown to contain $FeCO_3$ (identified by XRD in Figure 5) as well as products which contain a mixture of Cr, Fe and O. Similar to observations with X65, as O_2 content was increased to 1000 ppm, the quantity of $FeCO_3$ on the steel surface reduced significantly, as reflected in the intensity of the $FeCO_3$ peaks in the XRD patterns in Figure 5. The corroded sample in the presence of 1000 ppm O_2 (Figure 4(d)) also produced a cracked thin film which was rich in Cr, suggesting that the presence of O_2 resulted in the formation of a fragile or poorly adherent film. However, it is also possible that dehydration of the sample prior to analysis resulted in the presence of cracks (although this was not observed on other steel sample surfaces at lower O_2 contents).

Similar to carbon steel, there were no crystalline products detected on the surface of 5Cr in experiments containing 1000 ppm of O_2, yet a corrosion product is clearly identifiable on the steel surface in Figure 4(d). In support of these observations, Guo et al.[24] and Zhu et al.[25], found that the corrosion film on the surface of 3Cr steel exposed to CO_2-saturated water environments formed a Cr-rich amorphous layer which bears a similar resemblance to that observed in Figure 4(d). Such observations would explain why the XRD analysis in Figure 5 was unable to identify the nature of the corrosion product. The results from EDX analysis agree with the observations of Guo et al.[24] and Zhu et al.[25] in that the film observed is Cr-rich, containing a combination of Cr, Fe and O. The cracking of the film in Figure 4(d) also agrees with the work performed by Chen et al.[26] who showed that the Cr rich compound in their study was mainly in the form of chromium hydroxide ($Cr(OH)_3$) which is believed to dehydrate upon removal from the system, forming chromium oxide (Cr_2O_3).

The influence of O_2 on corrosion product formation

To further determine the role of O_2 in the corrosion behavior of X65 and 5Cr steel, XPS analysis was performed on both steel samples when exposed to the systems containing 1000 ppm O_2 in an effort to determine the corrosion products present. Figure 6 provides the high resolution XPS spectra for X65 and 5Cr samples. The elements of interest on both surfaces were Fe, O and Cr.

High resolution XPS analysis of both iron and chromium oxides/hydroxides is inherently challenging due to the complexity of their 2p spectra resulting from peak asymmetries, multiplet splitting and the uncertainly associated with closely overlapping binding energies. Therefore, due to the potential mix of iron and chromium oxides/hydroxides on the surface,

corroborating evidence from the O1s spectra were used to help support the analysis, although this also presented limitations, as will be discussed.

Referring to the X65 Fe2p binding energies in Table 3, the results suggest a mixed corrosion product consisting of Fe_2O_3, (indicating a number of peaks associated with multiplet splitting based on the work of Biesinger et al.[27]) and potentially FeOOH and/or Fe_3O_4, although this could not be confirmed due to overlapping binding energies and is unlikely given the fact that only 1 or 2 of the multiplet peaks were identified which all coincided with possible peaks associated with Fe_2O_3[27].

The results of O1s binding energies for X65 in Table 2 confirm the presence of Fe_2O_3 but are unable to confirm the additional presence of FeOOH and/or Fe_3O_4. No XPS spectra were observed for Cr, indicating that no Cr compounds were present in the corrosion product on X65, as expected in light of the very low Cr content within the steel.

The Fe2p and O1s scans for 5Cr reflect a similar composition of corrosion product compared to that of X65, confirming the presence of Fe_2O_3, along with the possible existence of Fe_3O_4. However, a noticeable difference exists in the Cr spectra between X65 and 5Cr with a $Cr2p_{3/2}$ peak emerging at 574.4 eV, corresponding to Cr. $Cr2p_{3/2}$ peaks are located at 576.3, 577.5 and 578.8 eV, corresponding to Cr_2O_3 and potentially $Cr(OH)_3$[27]. The development of this Cr-rich corrosion product detected on the surface of 5Cr has been identified by a number of authors[24, 25] and is believed to be one of the reasons behind low Cr-bearing steels offering improved corrosion resistance compare to X65 steel, particularly in higher temperature experiments.

Surface pitting analysis and its relation to film formation

Only a small number of publications have considered the extent of localized corrosion of carbon steels in environments typical of CO_2 transport[15, 23, 28]. To date, the influence of O_2 in particular on the localized corrosion behavior of dense phase CO_2 pipeline materials has not been systematically studied, yet the presence of O_2 is known to influence localized attack. The purpose of this work was to build on the research of previous authors and determine the effects of O_2 content on the propensity for localized/pitting corrosion to occur in dense phase $CO_2/O_2/H_2O$ systems. This was achieved through the implementation of white light interferometry using a precise multi-region analysis method.

Profilometry measurements extracted from the samples exposed to the water-saturated CO_2 environment at 35℃ and 80 bar with various concentrations of O_2 added to the system are provided in Figure 7. The localized corrosion rates are based on the top 10 deepest surface pits (converted into a penetration rate based on the duration of exposure to the system), in

alignment with ASTM Standard G46-94[29]. Figure 7 indicated that the localized attack on carbon steel is more extensive than that of 5Cr for all of the conditions evaluated. Perhaps the most significant observation is the distinct increase in the rate of localized attack as O_2 content is increased. Based on an exposure time of 48 hours, the localized corrosion rate was recorded at 0.9 mm/year in the absence of O_2 and increased to in excess of 3 mm/year at 1000 ppm O_2 for X65 steel. In contrast, the localized corrosion rate of 5Cr increased from 0.3 mm/year to 2.2 mm/year.

Typical profilometry images indicating the extent of the attack are provided in Figure 8, which demonstrate the influence of O_2 on the pit morphology as well as the depth of penetration. In publications by Schmitt[10, 30] the presence of small concentrations of O_2 can make Cr-containing steels more susceptible to localized corrosion and this is reflected in the profilometry measurements performed within this study. The SEM images in Figure 4 also suggest that increasing O_2 content appears to make the corrosion film more fragile, causing local disruption which could potentially be related to the increase in localized attack observed. In another study, Rosli et al.[12] observed that O_2 was actually capable of degrading $FeCO_3$ on steel surfaces, replacing the film with iron oxide/hydroxide tubercles. These tubercles possessed a nodule-like structure and effectively shielded part of the metal, reducing O_2 availability to that area. This was believed to result in the establishment of a galvanic cell consisting of an anode within the tubercle, surrounded by a large cathodic surface, causing accelerated attack under the tubercle and leading to localized corrosion. Although not confirmed in this study, it is possible the heterogeneous surface caused by the presence of O_2 may have led to O_2 deficiency locally on the steel surface, resulting in the establishment of local galvanic cells, leading to accelerated localized corrosion.

It is interesting to note that both X65 and 5Cr steels display similar corrosion behavior in the water-saturated dense phase CO_2 environment in the presence of increasing O_2 concentration. Both materials exhibited a decrease in general corrosion rate and an increase in the extent of localized attack with increasing O_2 content. These observations show there is a distinct change in the corrosion behavior when increasing O_2 content, with both materials shifting from a general corrosion process to a localized corrosion dominated mechanism.

In terms of the X65 steel, as O_2 concentration in the system increased, the formation of $FeCO_3$ inhibited as Fe^{2+} ions were oxidised to Fe^{3+}. This results in the formation of Fe_2O_3 (and potentially FeOOH and Fe_3O_4 based on the XPS results) on the steel surface. The formation of Fe_2O_3 specifically is generated through the following reaction:

$$2\mathrm{Fe} + O_2 + H_2O \rightarrow Fe_2O_3 + H_2 \quad (3)$$

It is also possible that the formation of the iron hydroxide/oxide corrosion products results in passivation/protection of the steel surface, as observed in bicarbonate/carbonate solutions by Kvarekval[13] which would explain the decrease in general corrosion with increased O_2 content. However, the passive/protective nature of the film cannot be confirmed in the absence of electrochemical measurements.

In the context of 5Cr, $FeCO_3$ is again observed in the absence of O_2 through XRD measurements, but the crystals exhibit a distinctly different morphology in comparison to those on the surface of X65. The corrosion product developed was also shown to contain traces of Cr. Nyborg[31] and Chen[26] showed that Cr-containing steels are capable of supressing pitting corrosion more effectively due to an increased level of Cr in the corrosion product layer. The Cr-containing corrosion product is believed to be able to reform more easily and exhibit improved cation selectivity, which would theoretically reduce the effects of localized attack compared to carbon steels, aligning with the observations in this work.

As O_2 content was increased in the presence of 5Cr, $FeCO_3$ film formation was again suppressed and the corrosion product film produced in the presence of 1000 ppm O_2 was shown to contain Cr_2O_3, Fe_2O_3 and potentially $Cr(OH)_3$, FeOOH and/or Fe_3O_4 based on XPS measurement. The presence of Cr_2O_3 can be ascribed the initial formation of $Cr(OH)_3$ followed by its dehydration, as suggested by Chen et al.,[26]:

$$Cr^{3+} + 3OH^- \rightarrow \mathrm{Cr}(OH)_3 \quad (4)$$

$$2\mathrm{Cr}(OH)_3 \rightarrow Cr_2O_3 + 3H_2O \quad (5)$$

Despite $FeCO_3$ being inhibited on both X65 and 5Cr surfaces, the general corrosion rate was reduced as O_2 concentration increased, along with an increase in localized attack. For both these materials, it is difficult to ascribe the reduction in general corrosion purely to the formation of the iron and or chromium oxides/hydroxides, although these have been shown to have exhibit passive-like behavior and could potentially protect the surface significantly whilst also contributing towards galvanic effects as a result of the film hetereogeneity, resulting in accelerated localized attack. This explanation would support both the decrease in general corrosion rate and the increase in localized attack with increasing O_2 content.

X65 and 5Cr samples exposed to under-saturated conditions with 1000 ppm of O_2

Experiments in the water-saturated CO_2 phase described previously revealed that corrosion of X65 and 5Cr can take place at the surface at 35 ℃ and 80 bar. However, considering the

conditions during the transport of CO_2 in pipelines, operators tend to dehydrate the CO_2 stream to specified levels below the solubility of water in the CO_2 prior to transport. Therefore, it was also important to study the behavior of X65 and 5Cr when exposed to under-saturated conditions in the supercritical CO_2 phase in the presence of 1000 ppm O_2 to determine the water content threshold required to avoid corrosion. For these series of tests, the operating conditions remained the same (80 bar and 35°C), while the water content was controlled at 2800, 1770, 1200, 650, 300 and 0 ppm.

The measured general corrosion rates of X65 and 5Cr when exposed to the under-saturated conditions at 35°C and 80 bar in the presence of 1000 ppm O_2 are provided in Figure 9. As the water content was increased from 0 ppm to water-saturated conditions, no measureable corrosion was recorded until a water content of 1200 ppm and 1770 ppm were reached for X65 and 5Cr, respectively. SEM images and photographs of the sample surfaces provided in Figure 10 (specifically (a) and (d) at 1200 ppm) corroborate with the mass loss measurements in that minimal corrosion is observed on X65 and no corrosion is visible on 5Cr. Relating these values to other observations in literature, Ruhl and Kranzmann[32] determined that at 100 bar CO_2 at 60°C and in the presence of 100 ppm O_2, no corrosion was observed when the water content was 400 ppm, agreeing with experimental results provided here is Figure 9. Furthermore, Dugstad et al.[15] evaluated the corrosion behavior of X65 steel at 100 bar and 20°C in liquid CO_2 in the presence of ~1220 ppm water with addition of 200 ppm O_2. From 30 day exposure experiments, the results indicated no corrosion occurred on carbon steel at all under these conditions, which agrees closely with the minimal corrosion rate of 0.002 mm/year recorded in Figure 9.

Localized corrosion rates for specimens in the presence of 1000 ppm O_2 at 35°C and 80 bar are provided in Figure 11. The level of pitting/localized attack on the steel surface is well over one order of magnitude greater than the general corrosion rates in all instances, showing that localized corrosion may represent a threat to the integrity of carbon steel pipelines involved in transporting water-containing supercritical CO_2 with 1000 ppm O_2 if the water content is substantial enough and pitting rates are maintained. However, the results show that if the water content at 35°C is 1200 ppm or below, then no localized corrosion will be observed for both X65 and 5Cr. Again, the results also agree with Dugstad et al.,[15] in that ~1200 ppm water produced no significant general or localized corrosion. The experimental work is also supported by Sim et al.[33] who evaluated localized corrosion rates of X65 steel at 80 bar and 40°C in the presence of different concentrations of water and reported localized corrosion rates which were also nearly one order of magnitude greater than the general thickness loss.

Figure 11 indicates that if the water content is increased to 2800 ppm, then the average pitting rate reaches 0.8 and 0.7 mm/year for carbon steel and 5Cr respectively, even though the system is under-saturated. When the CO_2 is completely saturated with water at 35°C, the average pitting rate rises significantly to 3.1 and 2.2 mm/year for X65 and 5Cr, in comparison to the general corrosion rates of 0.03 and 0.02 mm/year. It is important to stress that the predicted rates of localized attack are extrapolated from 48 hour tests and it is essential to determine whether the rate attack is maintained in longer duration experiments before the true risk to pipeline integrity can be quantified. The results within this work highlight the importance of quantifying localized corrosion rates and understanding the propagation of pits/localized attack in dense phase CO_2 systems to ensure appropriate impurity limits are established for CO_2 transport pipelines to guarantee their long term integrity.

CONCLUSIONS

The research presented has focused towards quantifying the extent of both general and localized corrosion of X65 carbon steel and 5Cr in water-containing supercritical CO_2 environments containing various concentrations of O_2 (0-1000 ppm), representative of dense phase CO_2 transport. Tests were conducted at a pressure of 80 bar and a temperature of 35°C for 48 hours. The main conclusions which can be drawn from this study are:

- In the water-saturated supercritical CO_2 environment, the average general corrosion rates for X65 carbon steel over 48 hours reduced from 0.10 mm/year to 0.03 mm/year when the O_2 concentration was increased from 0 ppm to 1000 ppm. The general corrosion rate of 5Cr also reduced from 0.13 mm/year to 0.02 mm/year over the same range of O_2 contents.

- O_2 inhibited the precipitation of $FeCO_3$ on the surface of X65 and 5Cr, promoting the formation of Fe_2O_3 (and potentially other oxides and hydroxides) in its place. The thin amorphous oxide layer of corrosion product appeared to offer improved protection in terms of general corrosion.

- The extent of localized attack observed became much more severe with increasing O_2 content from 0 to 1000 ppm. Addition of 500 ppm O_2 resulted in increasing the localized corrosion rates from 0.92 and 0.29 mm/year to 1.24 and 1.00 mm/year for X65 and 5Cr, respectively. The localized corrosion rates increased further to 3.13

444 and 2.20 mm/year as the O_2 content increases up to 1000 ppm for X65 and 5Cr. The
445 improved localized corrosion resistance between 5Cr and X65 was believed to be
446 attributed to the difference in corrosion product morphology. The corrosion product
447 on 5Cr was a Cr-rich film comprising of Cr oxides and/or hydroxides and Fe oxides
448 and/or hydroxides.
449
450 • Corrosion of carbon steel was shown to take place in conditions where the water
451 content is well below the solubility limit of water in supercritical CO_2 in the presence
452 of 1000 ppm O_2. However, no corrosion was observed below water contents of 1200
453 and 1770 ppm for X65 and 5Cr. Within these particular tests, 5Cr was shown to
454 withstand a higher humidity within the system before corrosion occurred, extending
455 the operating range in these particular conditions.
456
457 • The general corrosion rate on the steel surface was over one order of magnitude
458 smaller than the rate of surface pitting and the localized attack was shown to be
459 important in determining and quantifying the threat to CO_2 transport pipelines.
460
461
462
463
464

Reference

1. Sim, S., M. Cavanaugh, P. Corrigan, I. Cole, and N. Birbilis, Aqueous corrosion testing and neural network modeling to simulate corrosion of supercritical CO_2 pipelines in the carbon capture and storage cycle. Corrosion, 2013. 69(5): p. 477-486.
2. F. Ayello, K. Evans, R. Thodla, and N. Sridhar, "Effect of impurities on corrosion of steel in supercritical CO_2", in CORROSION 2010. 2010: San Antonio, TX:NACE.
3. Y.-S. Choi, S. Nešić, and D. Young, Effect of impurities on the corrosion behavior of CO_2 transmission pipeline steel in supercritical CO_2−water environments. Environmental Science & Technology, 2010. 44(23): p. 9233-9238.
4. Y. Hua, R. Barker, and A. Neville, Effect of temperautre on the critical water content for general and localised corrosion of X65 carbon steel in the transport of supercritical CO_2. The International Journal of Greenhouse Gas Control, 2014. 31: p. 48-60.
5. Y. Hua, R. Barker, C. T, M. Ward, and A. Neville, Relating Iron Carbonate Morphology to Corrosion Characteristics for Water-Saturated Supercritical CO_2 Systems. The Journal of Supercritical Fluids, 2014. vol. 98: p. 183-193.
6. Y. Hua, R. Barker, and A. Neville, Comparison of corrosion behaviour for X-65 carbon steel in supercritical CO_2-saturated water and water-saturated/unsaturated supercritical CO_2 The Journal of Supercritical Fluids, 2015. 97: p. 224-237.
7. A. Dugstad, B. Morland, and S. Clausen, Corrosion of transport pipelines for CO_2– Effect of water ingress. Energy Procedia, 2011. 4: p. 3063-3070.
8. Y.-S. Choi and S. Nesic, "Effect of water content on the corrosion behavior of carbon steel in supercritical CO_2 phase with impurities", in CORROSION 2011. 2011: Houston, TX:NACE.
9. Y.-S. Choi and S. Nešić, Determining the corrosive potential of CO_2 transport pipeline in high pCO_2–water environments. International Journal of Greenhouse Gas Control, 2011. 5(4): p. 788-797.
10. Schmitt, G. and R. Forster. Unexpected Effect of Small Oxygen Concentrations in Sales Gas on Element Currents between Pipeline Steel and Magnetite from Black Powder. in CORROSION 2015. 2015: NACE International.
11. S. Nesic, J. Postlethwaite, and S. Olsen, An electrochemical model for prediction of corrosion of mild steel in aqueous carbon dioxide solutions. Corrosion, 1996. 52(4): p. 280-294.
12. N. R. Rosli, Y. - S. Choi, and D. Young. Impact of Oxygen Ingress in CO_2 Corrosion of Mild Steel. in CORROSION 2014. 2014: NACE International.
13. Kvarekval, J., S. Olsen, and S. Skjerve. The effect of O_2 on CO_2 corrosion in pH stabilized gas/condensate pipelines. in CORROSION 2005. 2005: NACE International.
14. E.D. Visser, C. Hendriks, M. Barrio, M.J. MøInvik, G.D. Koeijer, S. Liljemark, and Y.L. Gallo, Dynamis CO_2 quality recommendations. International Journal of Greenhouse Gas Control, 2008. 2(4): p. 478-484.
15. A. Dugstad, M. Halseid, and B. Morland, Effect of SO_2 and NO_2 on corrosion and solid formation in dense phase CO_2 pipelines. Energy Procedia, 2013. 37: p. 2877-2887.
16. Y. M. Zeng, X. Pang, C. Shi, M. Arafin, R. Zavadil, and J. Collier. Influence of Impurities on Corrosion Performance of Pipeline Steels in Supercritical Carbon Dioxide. in CORROSION 2015. 2015: NACE International.
17. Kermani, B., J.C. Gonzales, G.L. Turconi, T.E. Perez, and C. Morales. In-field corrosion performance of 3% Cr steels in sweet and sour downhole production and water injection. in CORROSION 2004. 2004: NACE International.
18. Y. Hua, R. Barker, and A. Neville, Understanding the Influence of SO_2 and O_2 on the Corrosion of Carbon Steel in Water-Saturated Supercritical CO_2. Corrosion, 2014: p. Article In Press.

19. N. Spycher, K. Pruess, and J. Ennis-King, CO_2-H_2O mixtures in the geological sequestration of CO_2. I. Assessment and calculation of mutual solubilities from 12 to 100℃ and up to 600 bar. Geochimica et Cosmochimica Acta, 2003. 67(16): p. 3015-3031.
20. ASTM. Standard G1-03, Standard practice for preparing, cleaning, and evaluating corrosion test specimens. ASTM International: West Conshohocken, PA, 2003.
21. A. Dugstad and M. Halseid, Internal corrosion in dense phase CO_2 transport pipelines-state of the art and the need for further R&D. CORROSION 2012, 2012.
22. M. Halseid, A. Dugstad, and B. Morland, Corrosion and bulk phase reactions in CO_2 transport pipelines with impurities: review of recent published studies. Energy Procedia, 2014. 63: p. 2557-2569.
23. Sim, S., I.S. Cole, F. Bocher, P. Corrigan, R.P. Gamage, N. Ukwattage, and N. Birbilis, Investigating the effect of salt and acid impurities in supercritical CO_2 as relevant to the corrosion of carbon capture and storage pipelines. International Journal of Greenhouse Gas Control, 2013. 17(0): p. 534-541.
24. S.Q. Guo, L.N. Xu, L. Zhang, W. Chang, and M.X. Lu, Corrosion of Alloy Steels Containing 2% Chromium in CO_2 Environments. Corrosion Science, 2012. 63: p. 246-258.
25. J. Y. Zhu, L. N. Xu, and M. X. Lu, EIS study of the corrosion of 3Cr pipeline steel in simulated CO_2-saturated oilfield formation waters. Corrosion, 2015.
26. C. F. Chen, M. X. Lu, D. B. Sun, Z. H. Zhang, and W. Chang, Effect of chromium on the pitting resistance of oil tube steel in a carbon dioxide corrosion system. Corrosion, 2005. 61(6): p. 594-601.
27. M. C. Biesinger, B. P. Payne, A. P. Grosvenor, L. W. M. Lau, A. R. Gerson, and R. S. C. Smart, Resolving surface chemical states in XPS analysis of first row transition metals, oxides and hydroxides: Cr, Mn, Fe, Co and Ni. Applied Surface Science, 2011. 257(7): p. 2717-2730.
28. Y. Hua, R. Barker, and A. Neville, The influence of SO_2 on the tolerable water content to avoid pipeline corrosion during the transportation of supercritical CO_2. International Journal of Greenhouse Gas Control, 2015. 37: p. 412-423.
29. ASTM. Standard G46-94, Standard guide for examination and evaluation of pitting corrosion. ASTM International: West Conshohocken, PA, 2003.
30. Schmitt, G. and M. Horstemeier. Fundamental aspects of CO_2 metal loss corrosion-Part II: Influence of different parameters on CO_2 corrosion mechanisms. in CORROSION 2006. 2006: NACE International.
31. Nyborg, R. and A. Dugstad. Mesa Corrosion Attack in Carbon Steel and 0.5% Chromium Steel. in CORROSION 98. 1998: NACE International.
32. Ruhl, A.S. and A. Kranzmann, Investigation of Pipeline Corrosion in Pressurized CO_2 Containing Impurities. Energy Procedia, 2013. 37: p. 3131-3136.
33. S. Sim, F. Bocher, I.S. Cole, X.B. Chen, and N. Birbilis, Investigating the effect of water content in supercritical CO_2 as relevant to the corrosion of carbon capture and storage pipelines. Corrosion, 2014. 70(2): p. 185-195.
34. A. P. Grosvenor, B. A. Kobe, M. C. Biesinger, and N. S. McIntyre, Investigation of multiplet splitting of Fe 2p XPS spectra and bonding in iron compounds. Surface and Interface Analysis, 2004. 36(12): p. 1564-1574.
35. J. K. Heuer and J. F. Stubbins, An XPS characterization of $FeCO_3$ films from CO_2 corrosion. Corrosion Science, 1999. 41(7): p. 1231-1243.
36. Leveneur, J., D.F. Sanchez, J. Kennedy, P.L. Grande, G.V. Williams, J.B. Metson, and B.C. Cowie, Iron-based bimagnetic core/shell nanostructures in SiO2: a TEM, MEIS, and energy-resolved XPS analysis. Journal of Nanoparticle Research, 2012. 14(10): p. 1-9.
37. Abdel-Samad, H. and P.R. Watson, An XPS study of the adsorption of chromate on goethite (α-FeOOH). Applied Surface Science, 1997. 108(3): p. 371-377.
38. Maurice, V., S. Cadot, and P. Marcus, Hydroxylation of ultra-thin films of α-Cr_2O_3 (0001) formed on Cr (110). Surface Science, 2001. 471(1): p. 43-58.

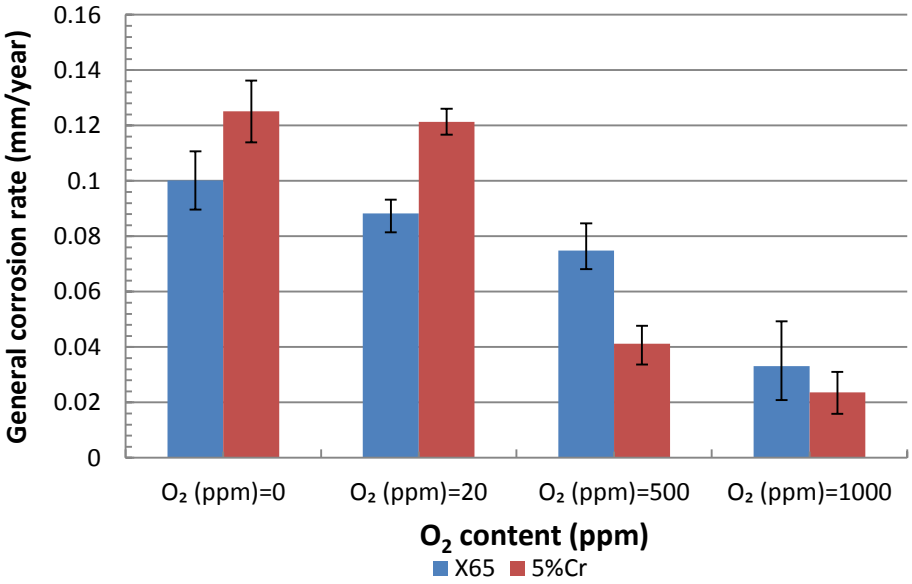

Figure 1: General corrosion rates of X65 carbon steel and 5Cr in water-saturated dense phase CO_2 at 80 bar and 35 °C for an exposure time of 48 hours at different O_2 concentrations (0, 20, 500 and 1000 ppm)

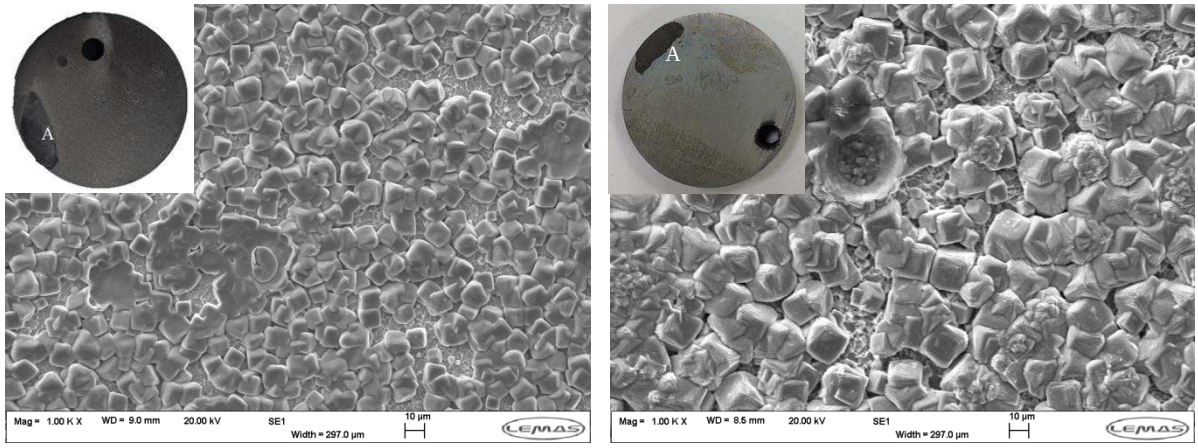

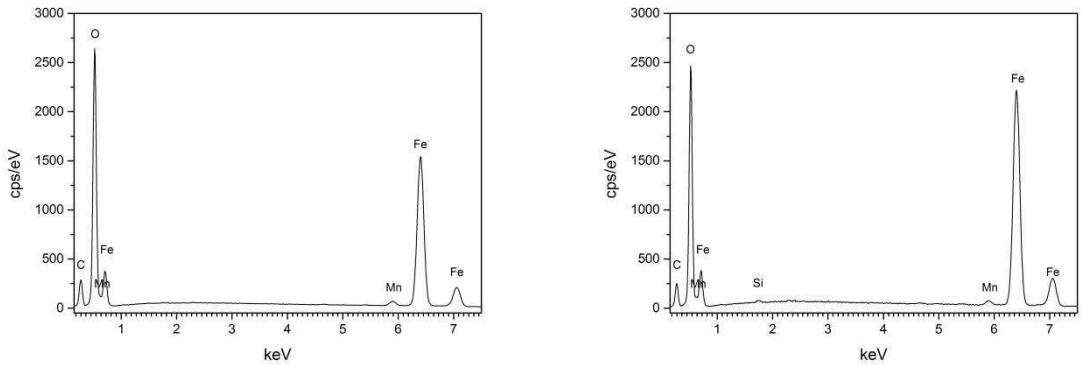

(a) (b)

581

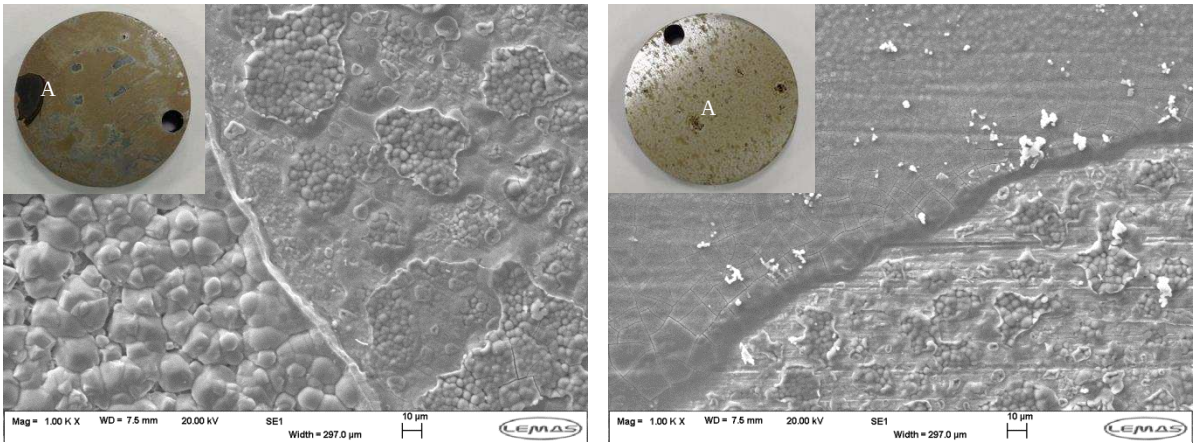

582

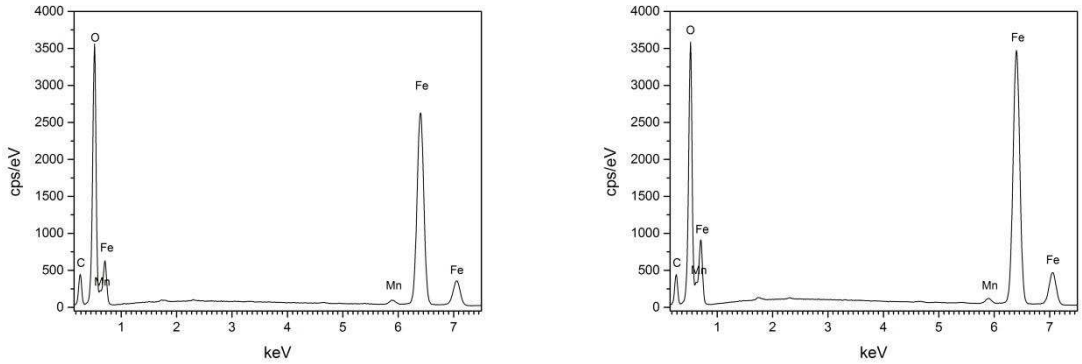

583 (c) (d)

584 **Figure 2: SEM images of X65 sample exposed to water-saturated dense phase CO_2**

585 **containing (a) 0 ppm O_2, (b) 20 ppm O_2, (c) 500 ppm and (d) 1000 ppm O_2 at 35℃ and**

586 **80 bar after 48 hours**

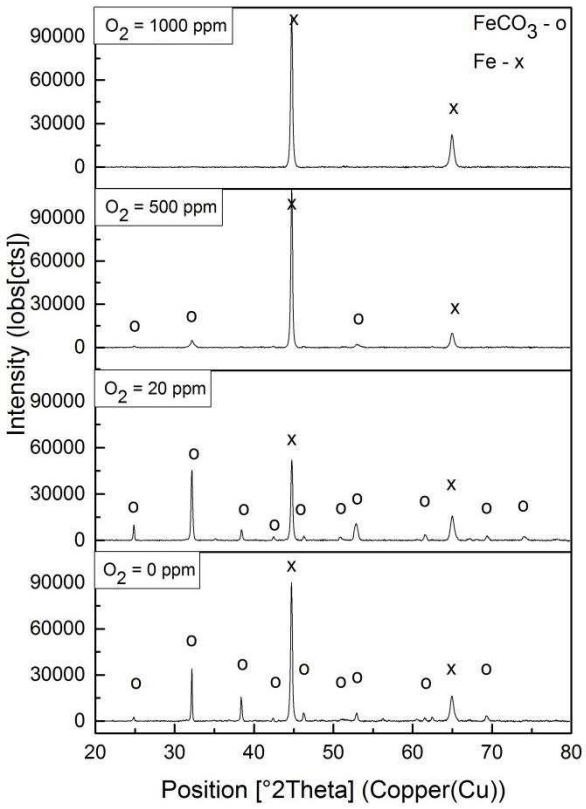

587

588 **Figure 3: XRD patterns of X65 samples exposed to water-saturated dense phase CO_2**
589 **containing 0, 20, 500 and 1000 ppm O_2 at 35°C and 80 bar after 48 hours**

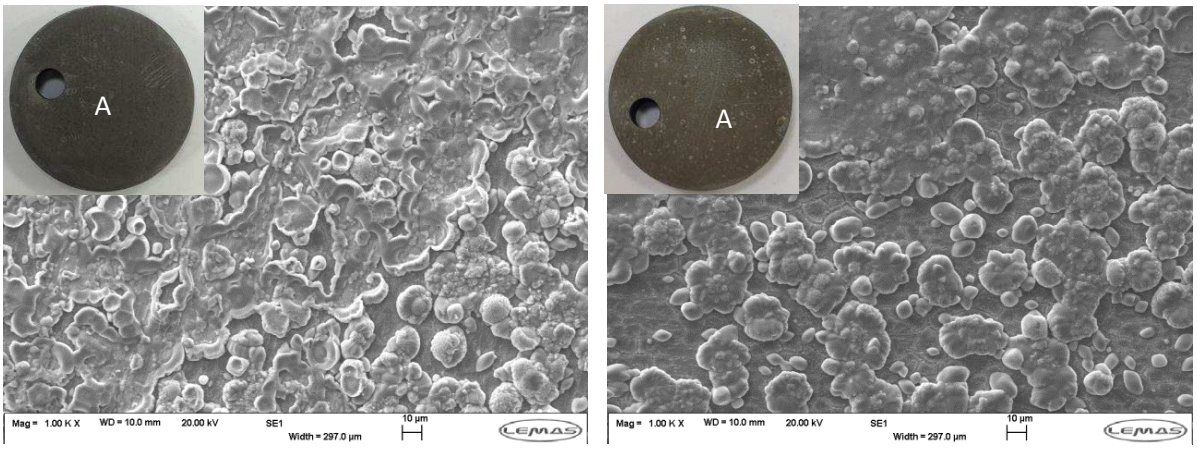

590

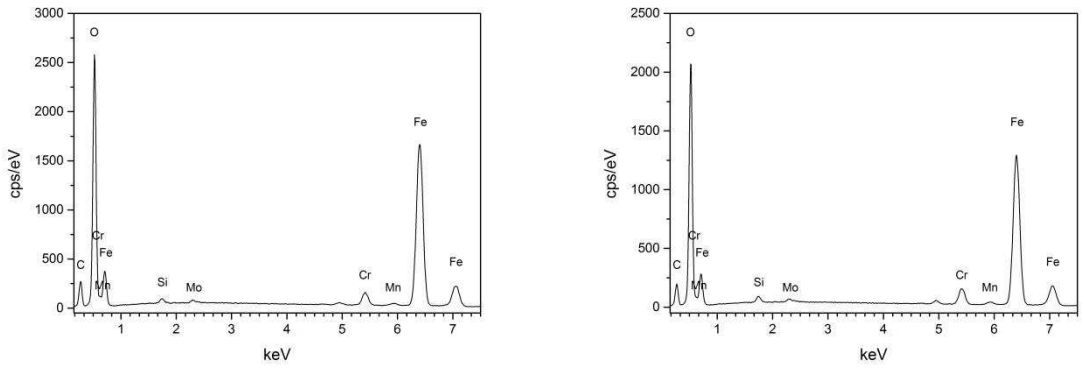

591
592 **(a)** **(b)**

593 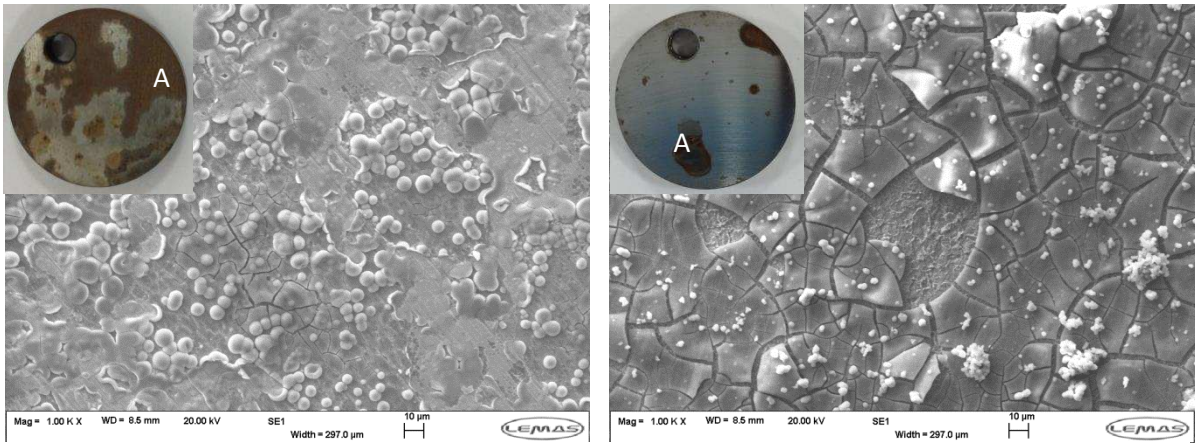

594 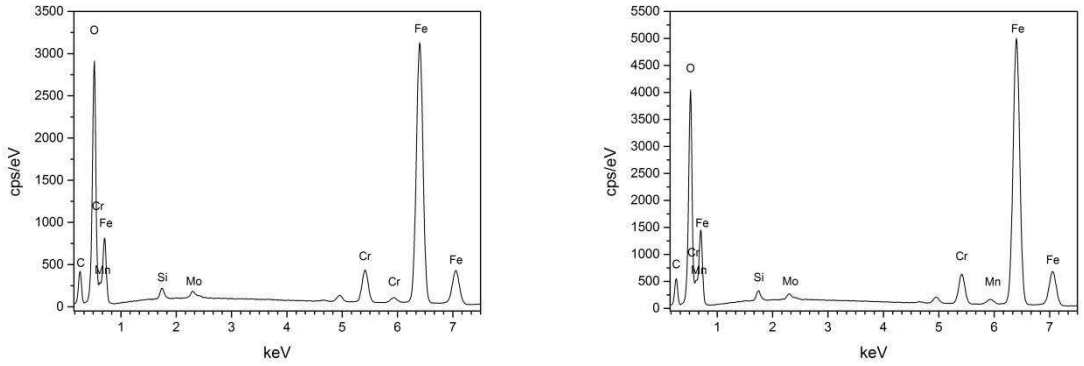

595 **(c)** **(d)**

596 **Figure 4: SEM images of 5Cr sample exposed to water-saturated dense phase CO_2**

597 **containing (a) 0 ppm O_2, (b) 20 ppm O_2, (c) 500 ppm and (d) 1000 ppm O_2 at 35℃ and**

598 **80 bar after 48 hours**

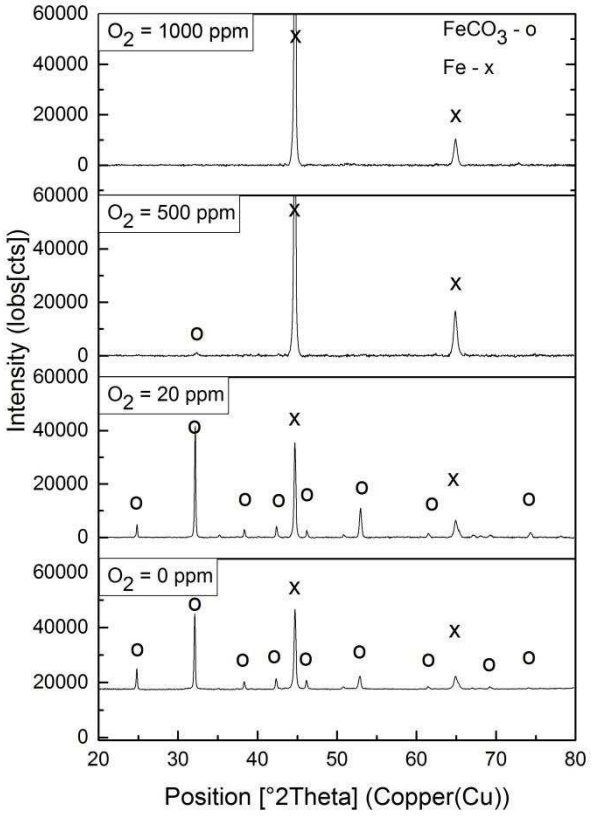

Figure 5: XRD pattern of 5Cr samples exposed to water-saturated dene phase CO_2 containing 0, 20, 500 and 1000 ppm O_2 at 35℃ and 80 bar after 48 hours

609

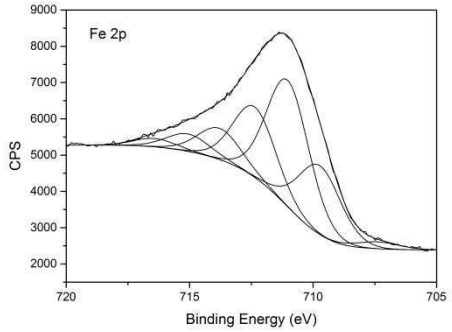

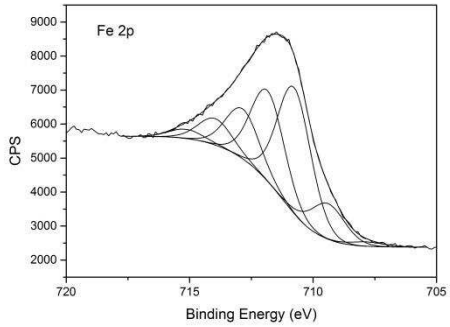

610

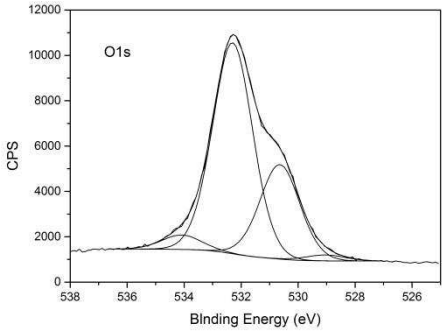

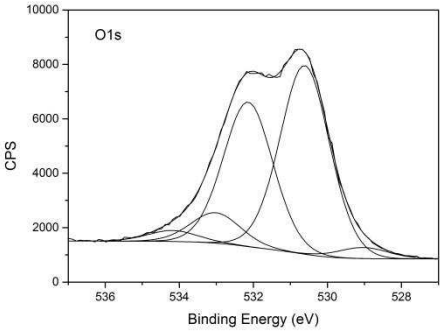

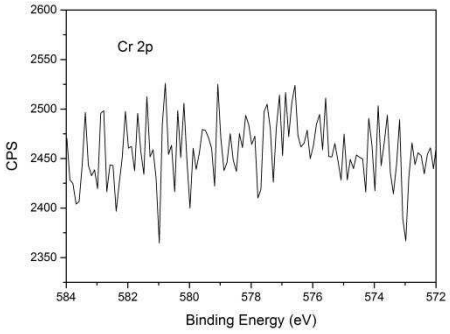

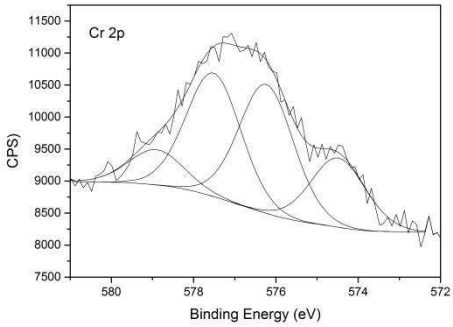

611 (a) (b)

612 **Figure 6: High resolution XPS scans on carbon steel (a) and 5Cr (b) samples exposed**
613 **to water-saturated environment in the presence of 1000 ppm O_2 after 48 hours.**

614

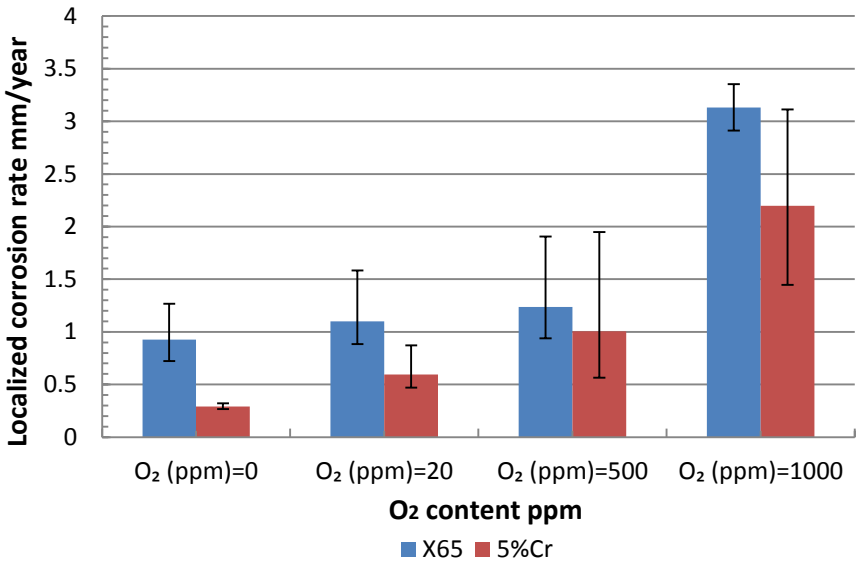

615

616 **Figure 7: Localized corrosion rates of X65 carbon steel and 5Cr in water-saturated**
617 **dense phase CO_2 at 80 bar and 35 ℃ for an exposure time of 48 hours at different O_2**
618 **concentrations (0, 20, 500 and 1000 ppm)**

619

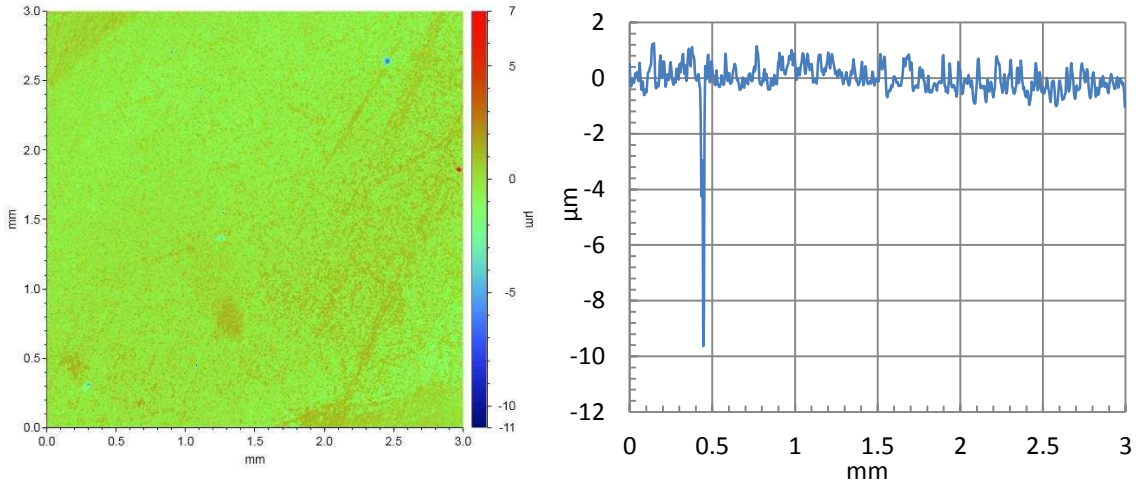

620

621 **(a)**

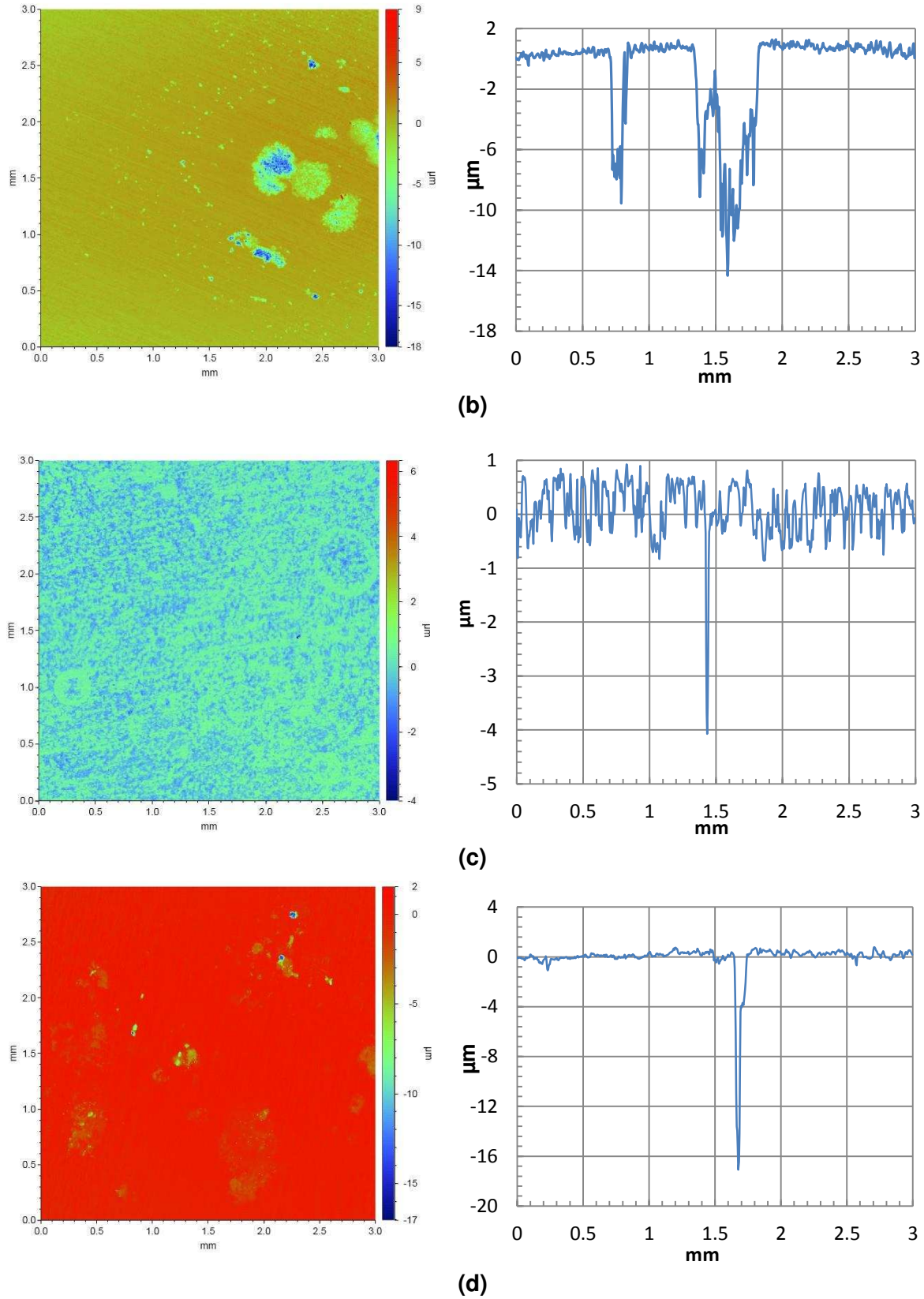

Figure 8: Example profilometry images of X65 and 5Cr samples exposed to water-saturated supercritical CO_2 environments containing varying concentrations of O_2 at 35°C and 80 bar for 48 hours (a) X65 - 0 ppm O_2, (b) X65 - 1000 ppm O_2 (c) 5Cr - 0 ppm O_2, and (d) 5Cr - 1000 ppm O_2

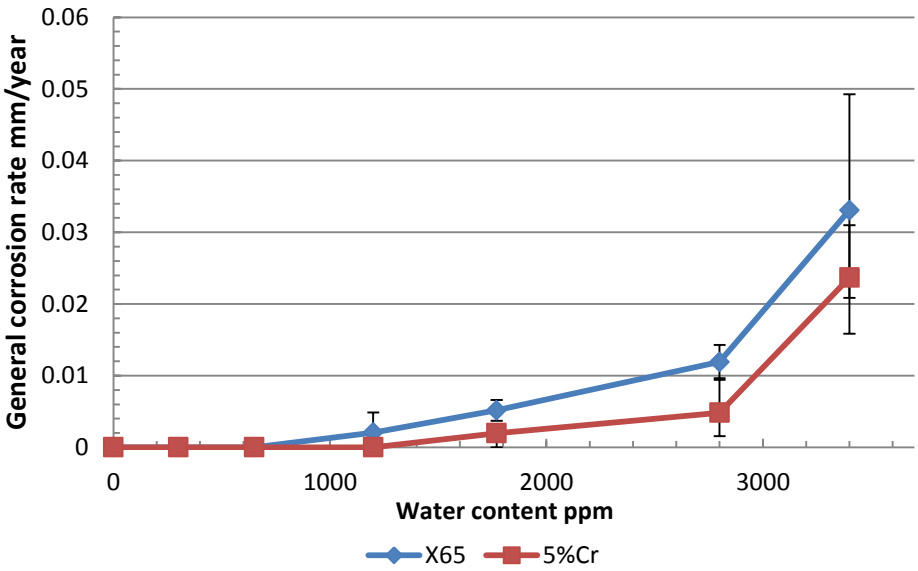

Figure 9: General corrosion rates of carbon steel and 5Cr in water-containing dense phase CO_2 in the presence of 1000 ppm O_2 at 80 bar and 35 ℃ for an exposure time of 48 hours

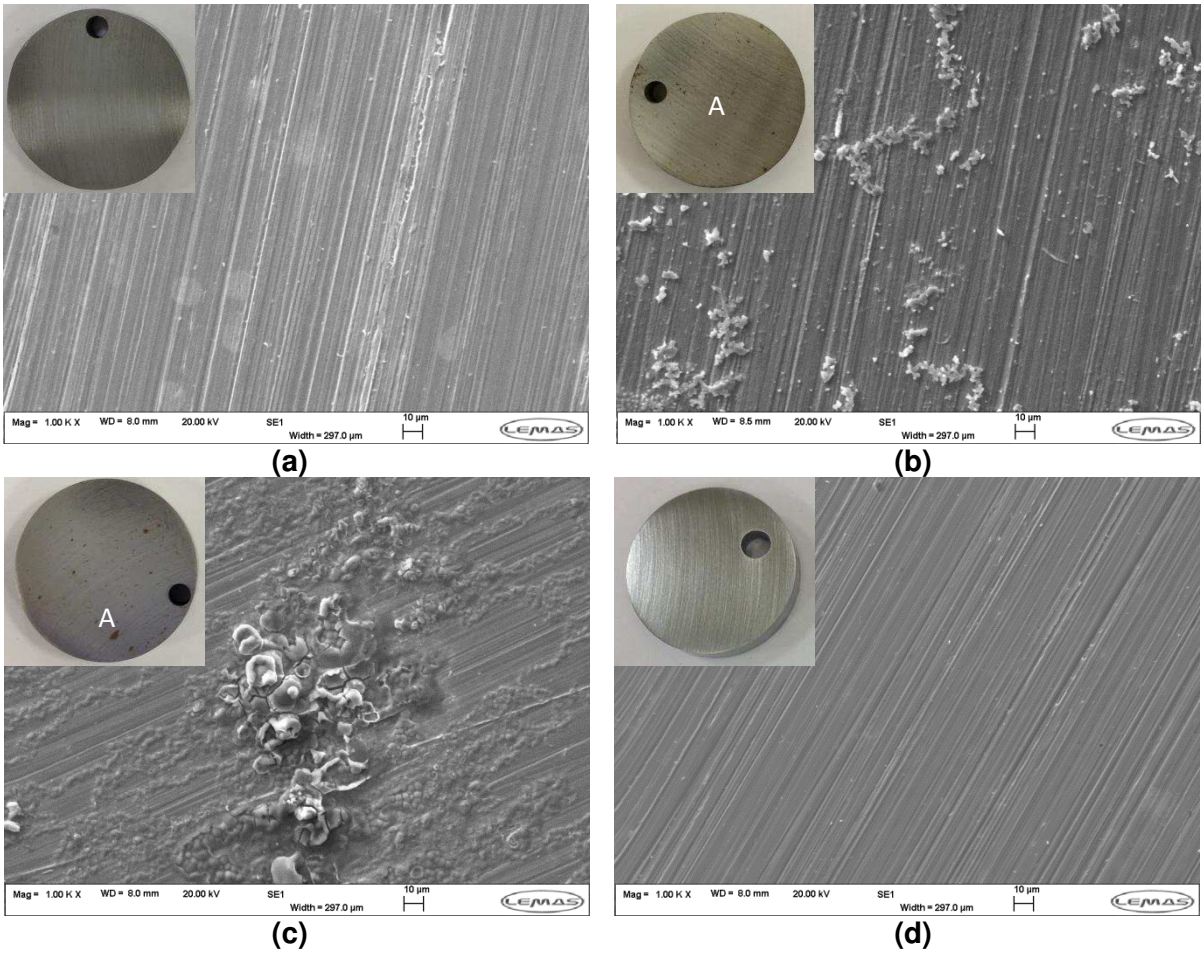

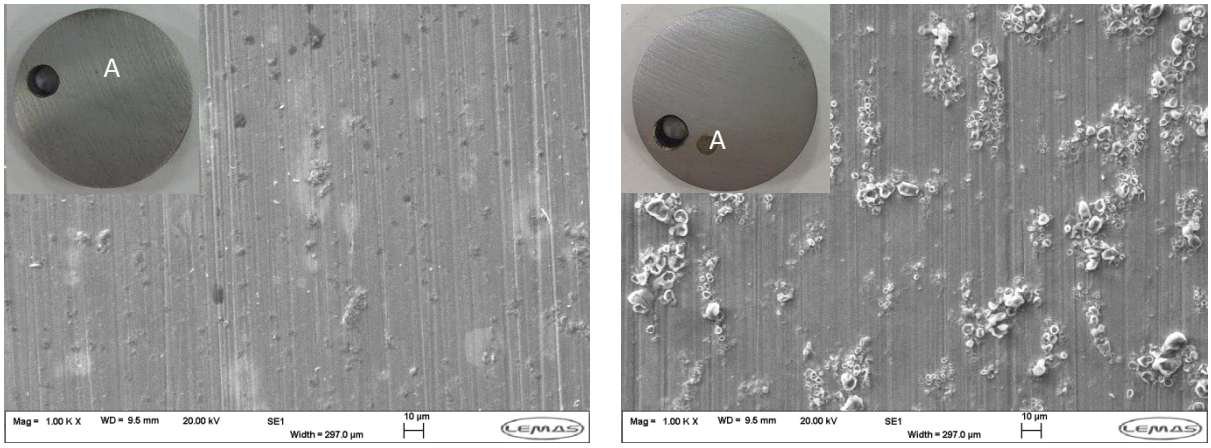

Figure 10: SEM images of X65 and 5Cr samples exposed to under-saturated dense phase CO_2 with 1000 ppm O_2 and water content of (a) 1200 ppm for X65, (b) 1770 ppm for X65, (c) 2800 ppm for X65 (d) 1200 ppm for 5Cr, (e) 1770 ppm for 5Cr and (f) 2800 ppm for 5Cr at 35 ℃ and 80 bar after 48 hours

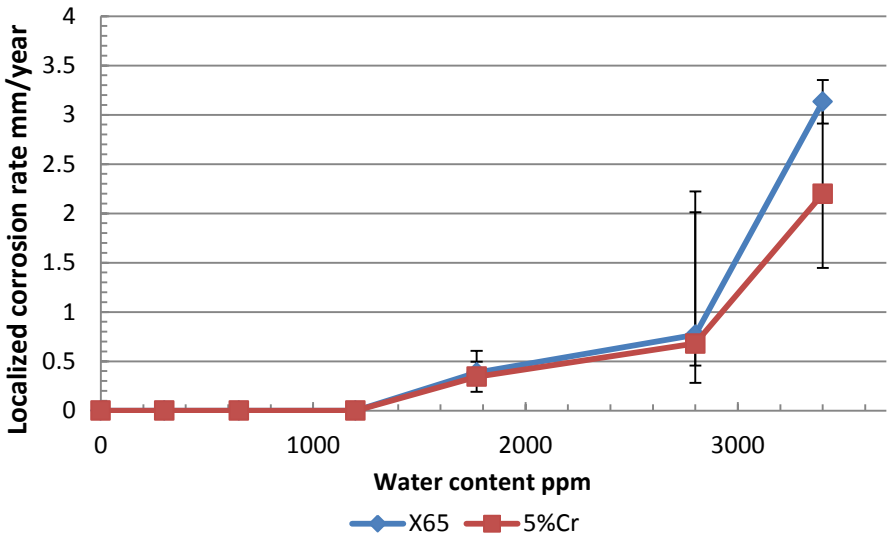

Figure 11: Localized corrosion rates of carbon steel and 5Cr in water-containing dense phase CO_2 in the presence of 1000 ppm O_2 at 80 bar and 35 ℃ for an exposure time of 48 hours

650

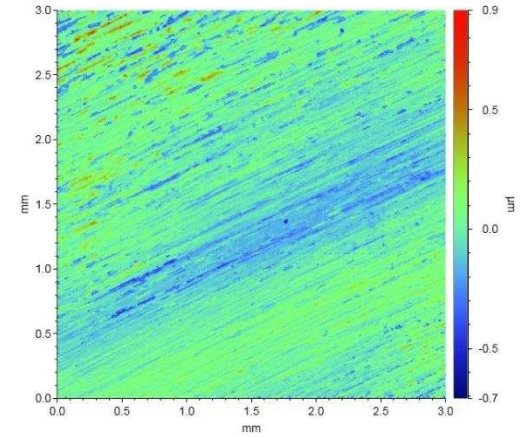

(a)

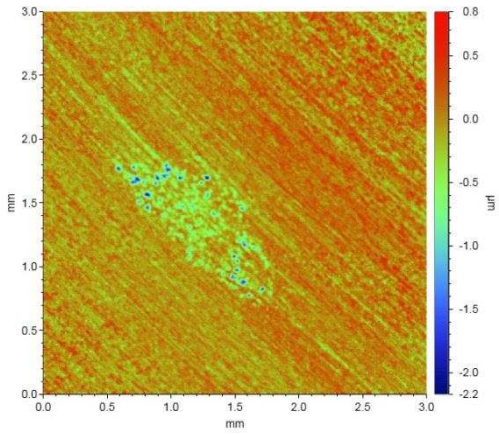

(b)

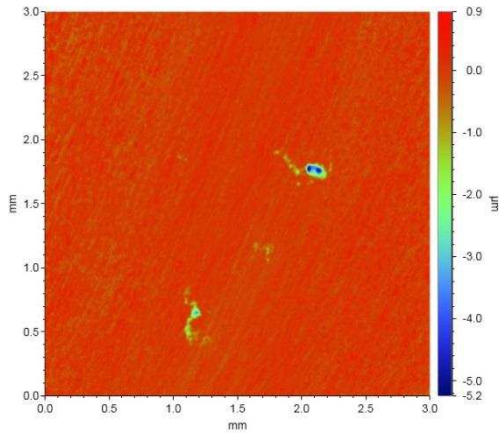

(c)

651

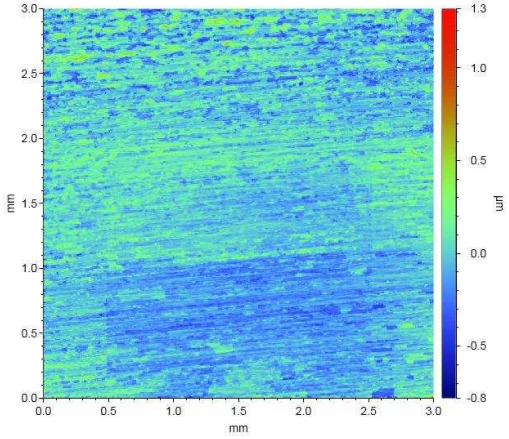

(a)

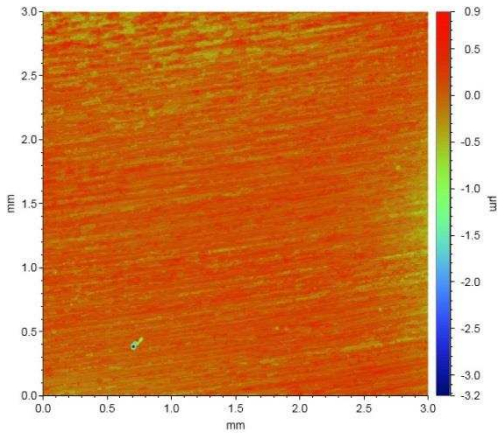

(b)

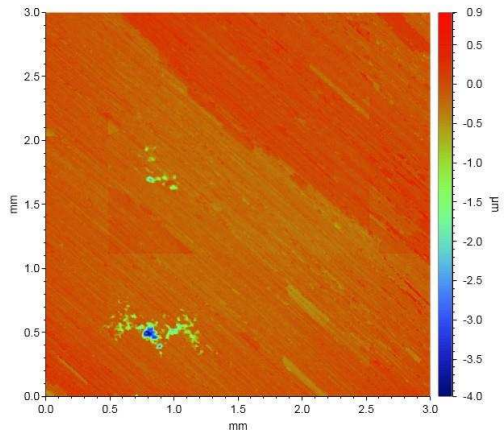

(c)

652 **Figure 12: Example profilometry images of X65 and 5Cr samples exposed to water-containing dense phase CO_2 with 1000 ppm O_2**
653 **and a water content of (a) 1200 ppm for X65, (b) 1770 ppm for X65, (c) 2800 ppm for X65 (d) 1200 ppm for 5Cr, (e) 1770 ppm for 5Cr**
654 **and (e) 2800 ppm for 5Cr at 35℃ and 80 bar after 48 hours**

655 **Table 1: Main elemental compositions of all the materials (wt.%)**

	X65	5Cr
C	0.12	0.38
Si	0.18	1.00
Mn	1.27	0.4
P	0.008	-
S	0.002	-
Cr	0.11	5.00
Mo	0.17	1.30
Fe	Balance	

656

657 **Table 2: Test matrix for corrosion experiments**

Water-saturated dense phase CO_2 experiments

Temperature (℃)	Pressure (bar)	Sample material	H_2O (ppm)	O_2 (ppm)	Immersion time (hours)
35	80	X65/5Cr	Above solubility limit of 3437 ppm through addition of 34000 ppm water	0, 20, 500 and 1000 ppm	48

Under-saturated dense phase CO_2 experiments (water content below solubility limit)

Temperature (℃)	Pressure (bar)	Sample materials	H_2O (ppm)	O_2 (ppm)	Immersion time (hours)
35	80	X65/5Cr	2800	1000	48
			1770		
			1200		
			650		
			300		

658

659

660

661

662

663 **Table 3: Binding energies of Fe2p, O1s, and Cr2p for X65 and 5Cr samples exposed to**
664 **water-saturated supercritical CO_2 conditions in the presence and absence of 1000**
665 **ppm O_2 at 35°C and 80 bar after 48 hours. All binding energies are accurate to within**
666 **±0.2eV or less based on 3 measurements per sample**

	X65 1000 ppm O_2	5Cr 1000 ppm O_2
Fe 2p	709.7 (Fe_2O_3)[27, 34, 35, 36, 37] 711.0 (Fe_2O_3)[34, 35] 712.4 (Fe_2O_3[34], Fe_3O_4[34] or FeOOH[34]) 713.7 (Fe_2O_3 or Fe_3O_4[27]) 714.9 (surface peak of Fe_2O_3[35])	707.8 (Fe[36]) 709.4 (Fe_2O_3[34]) 710.8 (Fe_2O_3[35]) 711.8 (FeOOH[27]) 712.9 (Fe_2O_3[27]) 713.9 (Fe_2O_3 or Fe_3O_4[27]) 715.1 (surface peak of Fe_2O_3[34, 35])
O1s	529.0 (Fe_2O_3[35]) 530.6 (hydroxyls on Fe_2O_3[35] or on Fe_2O_3/Fe_3O_4[37]) 532.3 (FeOOH or water[27]) 534.0 (water or contamination[27])	529.0 (Fe_2O_3 [35]) 530.6(hydroxyls on Fe_2O_3 or O^{2-} on $Fe_2O_3/Fe_3O_4/Cr_2O_3$[37]) 532.2 (FeOOH or water[27]) 533.1 (water or contamination[27, 36])
Cr 2p	-	574.4 (Cr[38]) 576.3 (Cr_2O_3 or $Cr(OH)_3$[27]) 577.5 (Cr_2O_3[27]) 578.8 (Cr_2O_3 or $Cr(OH)_3$[38])

667

668